Photodissociation of D 2 + induced by linearly chirped laser pulses

András Csehi, Gábor J. Halász, Lorenz S. Cederbaum, and Ágnes Vibók

Citation: The Journal of Chemical Physics **143**, 014305 (2015); doi: 10.1063/1.4923441
View online: http://dx.doi.org/10.1063/1.4923441
View Table of Contents: http://scitation.aip.org/content/aip/journal/jcp/143/1?ver=pdfcov
Published by the AIP Publishing

Photodissociation of D_2^+ induced by linearly chirped laser pulses

András Csehi,[1] Gábor J. Halász,[2] Lorenz S. Cederbaum,[3] and Ágnes Vibók[1]
[1]*Department of Theoretical Physics, University of Debrecen, P.O. Box 5, H-4010 Debrecen, Hungary*
[2]*Department of Information Technology, University of Debrecen, P.O. Box 12, H-4010 Debrecen, Hungary*
[3]*Theoretische Chemie, Physikalish-Chemisches Institut, Universität Heidelberg, H-69120 Heidelberg, Germany*

(Received 28 April 2015; accepted 23 June 2015; published online 7 July 2015)

Recently, it has been revealed that so-called light-induced conical intersections (LICIs) can be formed both by standing or by running laser waves even in diatomic molecules. Due to the strong nonadiabatic couplings, the existence of such LICIs has significant impact on the dynamical properties of a molecular system. In our former studies, the photodissociation process of the D_2^+ molecule was studied initiating the nuclear dynamics both from individual vibrational levels and from the superposition of all the vibrational states produced by ionizing D_2. In the present work, linearly chirped laser pulses were used for initiating the dissociation dynamics of D_2^+. In contrast to the constant frequency (transform limited) laser fields, the chirped pulses give rise to LICIs with a varying position according to the temporal frequency change. To demonstrate the impact of these LICIs on the dynamical properties of diatomics, the kinetic energy release spectra, the total dissociation probabilities, and the angular distributions of the D_2^+ photofragments were calculated and discussed. © *2015 AIP Publishing LLC.* [http://dx.doi.org/10.1063/1.4923441]

I. INTRODUCTION

The present paper is devoted to the theoretical description of the photodissociation dynamics of the D_2^+ molecule in the presence of a light-induced conical intersection (LICI) created by chirped laser pulses. Before summarizing the concept of LICIs,[1–11] let us briefly discuss the essence of the so-called "natural" conical intersections (CIs). As is well known from numerous important studies, CIs are always present in polyatomics and play a fundamental role in the dynamics of molecular systems.[12–22] In the vicinity of CIs, the Born–Oppenheimer approximation breaks down as the adiabatic potential energy surfaces become degenerate and the nonadiabatic coupling has singularity. In such situations, the nuclear and electronic motions couple and the energy exchange between electrons and nuclei can become significant. Thus, CIs act as efficient channels for ultrafast interstate crossings typically on a femtosecond time scale.

It is known that a molecular system must have at least two independent nuclear degrees of freedom so as to form a CI. Therefore, having only one nuclear degree of freedom in a molecule (for example, diatomics), CIs can never appear. However, if an additional degree of freedom is associated with the system due to some interaction with an environment (this is the situation, for example, in the case of laser-molecule interaction), then CIs can be formed. It was pointed out in previous papers[1,2] that CIs can be created both by running or by standing laser waves even in diatomics. The rotation of the molecules exposed to strong laser fields can serve as an additional degree of freedom because the interaction of the transition dipole moment of the system with the electric field leads to an effective torque toward the polarization direction of the light. In the correct dynamical description, one has to explicitly include this light-matter interaction into the Hamiltonian, and the change of nuclear dynamics due to the external laser field can be considered as arising from the appearance of a LICI. The positions of these LICIs are determined by the laser frequency and the strengths of their nonadiabatic couplings by the intensity of the laser. It has been demonstrated in several former theoretical works that LICIs have strong impact on the spectroscopic[2] and dynamical properties of diatomics.[4–11] Motivated by these theoretical predictions on the LICIs in diatomics, recent experiments on the laser-induced isomerization and photodissociation of polyatomic molecules[23,25,26] were qualitatively interpreted with the help of the concept of LICIs. The additional degrees of freedom in polyatomic molecules add much to the richness of the phenomenon of LICIs and open the door to its exploitation, as has been shown in Ref. 24.

The photodissociation process of the D_2^+ molecule has been thoroughly investigated for more than quarter of a century.[27–53] In our recent works, we have also discussed the dissociation dynamics of the D_2^+ molecule in the LICI framework starting the initial nuclear wave packet either from different vibrational eigenstates or from the Franck–Condon (FC) distribution of the vibrational states as can be obtained by first photoionizing D_2. One-dimensional (1d) and two-dimensional (2d) calculations have been performed and compared to each other. In the 1d model, the molecular rotational angle is only a parameter, i.e., the LICI was not taken into account, while in the 2d scheme, the rotational angle is assumed as a dynamic variable and, therefore, the LICI is explicitly included. The obtained 1d and 2d results strongly differ from each other, demonstrating the significant signature of the LICI on the dissociation dynamics of D_2^+.

So far laser pulses with only constant frequency were applied in the numerical simulations, and, therefore, the position of the LICI never changed during the dynamical process. This study goes beyond our former investigations as it uses linearly chirped laser pulses forming LICI with continuously changing position. The dissociation process of the D_2^+ molecule

is studied by solving the nuclear Schrödinger equation for both the 1d and 2d models. One of the purposes of the present work is to understand more deeply to what extent the behavior of the transform limited (TL) and "chirped" LICIs is different from each other. The other purpose is to investigate the influence of the chirped LICI on the kinetic energy release spectra (KER) and on the angular distributions of the photofragments.

We note here that the photodissociation process of the D_2^+ molecule by using chirped laser pulses has already been investigated experimentally.[47,54]

The paper is organized as follows. In Section II, the methodology and the physical background of the dynamical calculations are explained. Section III shortly discusses the applied electric field, the evolution of the nuclear wave packet by using the multi configuration time-dependent Hartree (MCTDH) method and the computational details including the physical quantities to be computed. The results on the kinetic energy release spectra, on the total photodissociation probabilities, as well as on the angular distributions and their interpretation are presented in Section IV. Section V briefly provides the conclusions and the perspectives.

II. METHODOLOGY AND PHYSICAL BACKGROUND

In this section, a brief description of D_2^+ will be given considering the low-lying electronic states, the corresponding transition dipole moment and the nuclear Hamiltonian. Furthermore, the definition of the applied chirped laser pulses will be discussed along with the useful technique that has been used for the propagation of the nuclear wave packets on the electronic surfaces.

Let us consider the electronic ground ($V_1 = 1s\sigma_g$) and first excited ($V_2 = 2p\sigma_u$) energy levels of the D_2^+ ion (see Fig. 1). These are the eigenstates of the field-free Hamiltonian. Next, we assume that the neutral D_2 molecule is suddenly ionized at $t = 0$. In this case, the vibrational ground state of the neutral molecule has been transferred vertically to the potential energy curve of the ground electronic state ($V_1 = 1s\sigma_g$) of the ion. It serves as the initial wave packet, which can be considered as the superposition of all the vibrational states of D_2^+. This FC distribution of the vibrational states of the ion has been used in most of our simulations. In some cases, we assume a different initial condition, where the ion is in a specific ro-vibrational state of its ground electronic ($1s\sigma_g$) state. To continue, we excite the $1s\sigma_g$ ground electronic state of the D_2^+ molecule by a resonant laser pulse to the repulsive $2p\sigma_u$ state (see also Fig. 1). As a result of this process, these two electronic states are radiatively coupled by the laser light. The respective non-vanishing transition dipole matrix element is responsible for this light-induced electronic transition. In the space of these two electronic states, the following time-dependent Hamiltonian holds for the ro-vibronic nuclear motions:

$$H = \begin{pmatrix} -\frac{1}{2\mu}\frac{\partial^2}{\partial R^2} + \frac{L_{\theta\varphi}^2}{2\mu R^2} & 0 \\ 0 & -\frac{1}{2\mu}\frac{\partial^2}{\partial R^2} + \frac{L_{\theta\varphi}^2}{2\mu R^2} \end{pmatrix} + \begin{pmatrix} V_1(R) & -E(t)\, d(R)\cos\theta \\ -E(t)\, d(R)\cos\theta & V_2(R) \end{pmatrix}. \quad (1)$$

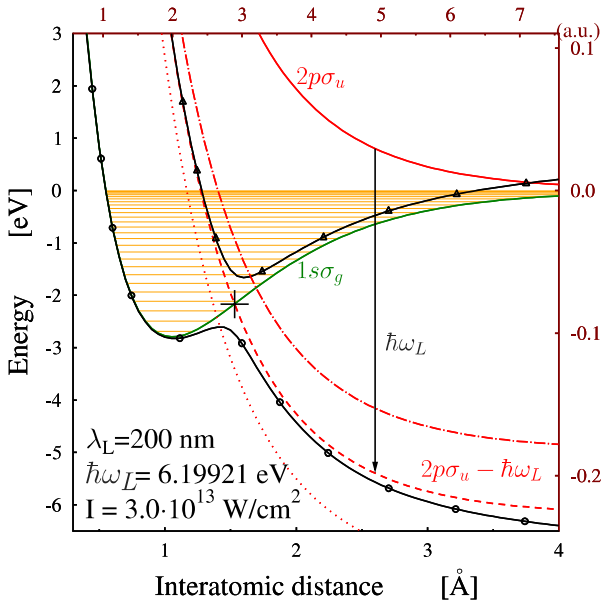

FIG. 1. A cut through the potential energy surface of the D_2^+ molecule as a function of interatomic separation. Diabatic energies of the ground ($1s\sigma_g$) and the first excited ($2p\sigma_u$) states are displayed with solid green and red lines, respectively. The field dressed excited states ($2p\sigma_u - \hbar\omega_L$) are presented for three different chirp situations (transform limited, dashed red line; positively chirped, dotted red line; negatively chirped, dashed-dotted red line). These field dressed excited states ($2p\sigma_u - \hbar\omega_L$) form light induced conical intersections (LICIs) with the ground state. Only for the case of a transform limited laser frequency $\omega_L = 6.199$ eV and field intensity of 3×10^{13} W/cm^2, a cut through the adiabatic surfaces at $\theta = 0$ (parallel to the field) is also shown by solid black lines marked with circles (V_{lower}) and triangles (V_{upper}). For the transform limited case, we denote with a cross the position of the LICI ($R_{LICI} = 1.53$, Å = 2.891 a.u., and E_{LICI} = −2.166 11 eV).

Here, R and (θ, φ) are the molecular vibrational and rotational coordinates, respectively, μ is the reduced mass, and $L_{\theta\varphi}$ is the angular momentum operator of the nuclei. One of the rotational coordinates, θ, represents the angle between the internuclear axis and the laser polarization. $V_1(R)$ ($1s\sigma_g$) and $V_2(R)$ ($2p\sigma_u$) are the energies of the two coupled electronic states. The laser field is characterized by its electric field $E(t)$ and $d(R)\left(= -\left\langle \psi_1^e \left| \sum_j r_j \right| \psi_2^e \right\rangle\right)$ is the transition dipole matrix element ($e = m_e = \hbar = 1$; atomic units are used throughout the article). The potential energies $V_1(R)$ and $V_2(R)$ and the transition dipole moment were adopted from Refs. 55 and 56. The essence of the LICI phenomenon can easily be demonstrated in the framework of the Floquet representation of the nuclear Hamiltonian (see Refs. 4 and 7 for a detailed discussion). This presentation provides a very illustrative picture and is often used to explain various phenomena in the area of strong field physics. After absorption of one photon, the energy of the ground electronic state is shifted upwards or equivalently, the $2p\sigma_u$ repulsive excited potential curve is shifted downwards by $\hbar\omega_L$ — where ω_L is the laser frequency — and a crossing between the diabatic ground and excited potential energy curves is formed. New light-induced adiabatic states V_{lower} and V_{upper} (Fig. 1) are obtained after diagonalizing the diabatic potential energy matrix (Eq. (1)). These two surfaces can cross each other, creating a conical intersection whenever the conditions $\cos\theta = 0$, $(\theta = \pi/2)$, and $V_1(R) = V_2(R) - \hbar\omega_L$ are simultaneously fulfilled.[1,2]

In contrast to the situation provided by natural CIs of field-free molecules, the LICI is controllable in the sense that the laser frequency determines its position in nuclear coordinate space and energy and the laser intensity the strength of the couplings. Increasing the frequency moves the CI to a smaller internuclear distance and to a lower energetic position while the opposite holds when decreasing the frequency.

III. COMPUTATIONAL DETAILS

In this section, we describe briefly the time-dependent electric field of the applied laser pulses, the theoretical approach used to compute the time evolution of the nuclear wave packets, and the physical quantities which are under investigation.

A. The applied electric field

During the calculations, Gaussian pulse with linear polarized time-dependent electric field along the x direction[63,64] was applied. We define the electric field as the derivative of a Gaussian shaped vector potential,

$$E(t) = -\frac{\partial}{\partial t} A(t), \tag{2}$$

where $A(t)$ is the vector potential,

$$A(t) = \frac{-\epsilon_0}{\sqrt[4]{1+\beta^2}} \cdot \sin\left\{\omega_0 \cdot (t-t_0) - \frac{\alpha}{2}(t-t_0)^2 + \varphi_0\right\} \cdot e^{-\frac{2\cdot\log 2}{1+\beta^2}\left(\frac{t-t_0}{T_p}\right)^2}. \tag{3}$$

Here, ϵ_0 is the maximum amplitude of the electric field, ω_0 is the carrier frequency of the laser pulse, T_p is the TL temporal pulse duration in terms of full width at half maximum (FWHM), t_0 is the time of the peek intensity, φ_0 is the carrier envelope phase (CEP) — which was kept 0 in this study, and the α and β parameters read

$$\begin{aligned} \alpha &= a \cdot \frac{\omega_0}{T_p}/(1+\beta^2), \\ \beta &= \frac{a \cdot \omega_0 \cdot T_p}{4 \cdot \log 2}, \end{aligned} \tag{4}$$

where a is the chirp parameter in terms of the relative change of the carrier frequency during the pulse. As seen in Eq. (3), we use here a linearly chirped pulse with frequency $\omega = \omega(t) = \omega_0 - \alpha\,(t - t_0)$. Other forms are also possible but will not be studied here. This parametrization has the following features: (i) the time integral of the electric field is zero, which is an intrinsic property of real pulses;[57] (ii) the spectra of the transform limited and the chirped pulses are the same; (iii) the frequency changing rate $|\alpha|$ is maximal for $|\beta| = 1$: $|\alpha|_{max} = 2\log 2/T_p^2$; and (iv) for the case of $|\beta| \ll 1$, the change of the carrier frequency during the pulse is proportional to the parameter a and to the central frequency: $\Delta\omega = \alpha \cdot T_p \cong a \cdot \omega_0$. The first three of these features are important characteristics of realistic linearly chirped pulses.

In the case of simulations starting from a FC distribution, we will refer to the time of the peak intensity as the delay time: $t_{delay} = t_0$ and the propagation starts at $t = 0$ fs. On the other hand, when our initial wave packet is one of the ro-vibrational eigenstates of the D_2^+ ion, the time of the peak intensity is chosen to be zero: $t_0 = 0$ and the propagation starts at $t = -100$ fs.

B. Time evolution of the nuclear wave packet

Studying the dissociation dynamics in the LICI framework, we have to solve the time-dependent nuclear Schrödinger equation (TDSE) with the Hamiltonian H described by Eq. (1). One of the most efficient approaches for this is the MCTDH method.[58–62] To characterize the vibrational degree of freedom, we have used FFT-DVR (Fast Fourier Transformation-Discrete Variable Representation) with N_R basis elements distributed within the range from 0.1 a.u. to 80 a.u. for the internuclear separation. The rotational degree of freedom was described by Legendre polynomials $\{P_J(\cos\theta)\}_{j=0,1,2,\ldots,N_\theta}$. These so called primitive basis sets (χ) were used to represent the single particle functions (ϕ), which in turn were used to represent the wave function,

$$\begin{aligned} \phi_{j_q}^{(q)}(q,t) &= \sum_{l=1}^{N_q} c_{j_q l}^{(q)}(t)\, \chi_l^{(q)}(q), \qquad q = R, \theta, \\ \psi(R,\theta,t) &= \sum_{j_R=1}^{n_R} \sum_{j_\theta=1}^{n_\theta} A_{j_R,j_\theta}(t) \phi_{j_R}^{(R)}(R,t) \phi_{j_\theta}^{(\theta)}(\theta,t). \end{aligned} \tag{5}$$

In the actual calculations, we have used $N_R = 2048$ and $N_\theta = 61$ or 199 (for the $v = 5$ and $v = 7$ cases). On both diabatic surfaces and for both degrees of freedom, a set of $n_R = n_\theta = 4, \ldots, 20$ single particle functions were applied to construct the nuclear wave packet of the system. (The actual value of N_θ and $n_R = n_\theta$ was chosen depending on the peak field intensity I_0.) It was tested that all calculations converged with these parameters.

C. Calculated quantities

The solution of the MCTDH equations with the ansatz in Equation (5) is used to calculate the KER $P_{KER}(E)$, the total dissociation probability P_{diss}, and the angular distribution $P(\theta_j)$ of the dissociation fragments. The KER of the photofragments reads[60]

$$P_{KER}(E) = \int_0^\infty dt \int_0^\infty dt' \langle\psi(t)|W|\psi(t')\rangle e^{-iE(t-t')}, \tag{6}$$

where $-iW$ is the complex absorbing potential (CAP) applied at the last 5 a.u. of the grid related to the vibrational degree of freedoms ($W = 0.002\,36 \cdot (r-75)^3$, if $r > 75$ a.u. on the dissociating surface) and

$$P(\theta_j) = \frac{1}{w_j} \int_0^\infty dt \langle\psi(t)|W_{\theta_j}|\psi(t)\rangle, \tag{7}$$

where $-iW_{\theta_j}$ is the projection of the CAP to a specific point of the angular grid ($j = 0, \ldots, N_\theta$), and w_j is the weight related to this grid point according to the applied DVR.

The total dissociation probability can be obtained as[60]

$$P_{diss} = \int_0^\infty dE \cdot P_{KER}(E). \tag{8}$$

Throughout the calculations, the initial nuclear wave function (at $t \ll 0\ fs$) was assumed to be in its rotational ground state ($J = 0$) and in the superposition of vibrational eigenstates or in one of its vibrational eigenstates ($\nu = 5; 7$). In the former case, the FC distribution of the vibrational states of the ion has been used. Initially, the molecules are thus assumed in the numerical calculations to be nonaligned and isotropically distributed and subject to linearly polarized Gaussian laser pulses centered around $t_0 = 0$–80 fs. The wavelengths and the pulse duration in FWHM are 200 nm and $t_{pulse} = 10$ fs (or 30 fs in some cases), respectively. Several different intensity values of the exciting laser pulse have been employed ranging from 1×10^9 to 1×10^{14} W/cm^2. The parameters of the calculations are $a = 0, \pm 0.03, \pm 0.008$ for transform limited and for chirped laser pulses, respectively. For the applied pulse durations (10 and 30 fs) and a values, the β parameters are close to ± 1, and consequently, the frequency changing rate (α) is close to its maximal possible value.

To demonstrate the impact of the laser induced conical intersection on the dissociation process of D_2^+, we compare the results obtained from the full 2d model in which both the rotational and vibrational coordinates are accounted as dynamical variables with 1d calculations where the rotational degree of freedom (θ) is used only as a parameter and accordingly the LICI is not considered. In the 1d situation, the ion's initial orientation is not changing during the dissociation and the "effective field strength" was the projection of the real field on the axis of the molecule: $\varepsilon_0^{eff} = \varepsilon_0 \cos\theta$ (i.e., with an effective intensity of $I_0^{eff} = I_0 \cos^2\theta$).

IV. RESULTS AND DISCUSSION

As mentioned in the Introduction, our aim is to investigate to what extent the time-dependent frequency of the resonant laser pulse changes the dynamical evolution of the photodissociation process of the D_2^+ ion. To see some effects quantitatively, calculations have been performed both with chirped and with TL laser pulses over a wide range of intensities and delay times for the KER, for the total dissociation probability and for the angular distribution of the molecular fragments. Throughout the paper, a $\lambda = 200$ nm wavelength ($\hbar\omega_L = 6.199$ eV) was applied for the TL pulse and also for the central value of the negatively and positively chirped pulses.

Figure 2 (panel (a)) shows the 2d total dissociation probability (Eq. (8)) as a function of time delay for the TL and for the chirped simulations employing a 10 fs laser pulse. The initial nuclear wave packet is built up as the FC distribution of the ionic vibrational states and its field-free time evolution can be visualized in Fig. 2 (panel (b)). The first conspicuous result is that the period of the total dissociation yield curves (panel (a)) is replicas of the field-free molecular vibration curve (panel (b)). This is mainly because the dissociation rate increases if the nuclear wave packet is moving forward to the direction of

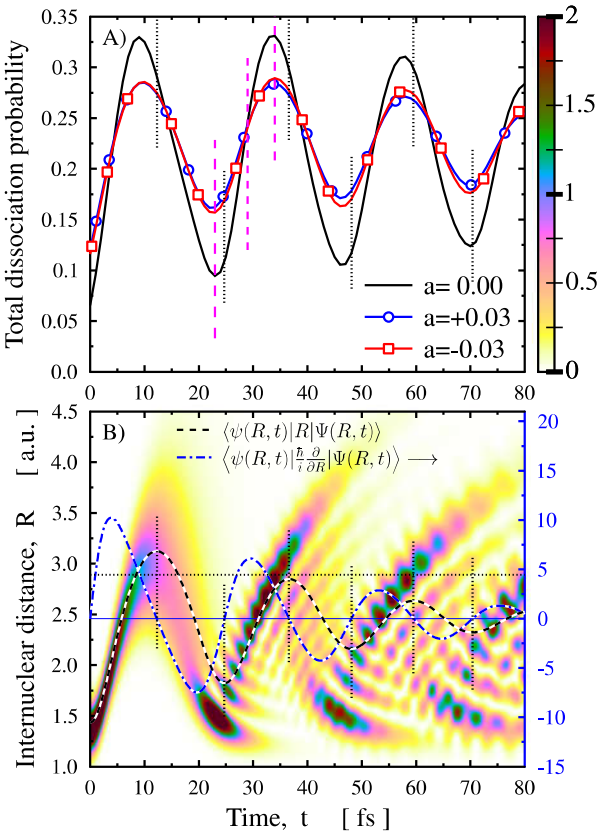

FIG. 2. Total dissociation probability as a function of delay time at 1×10^{13} W/cm^2 intensity (panel (a)). Shown are the results for the transform limited $a = 0$, negatively chirped $a = -0.03$ (square), and positively chirped $a = 0.03$ (circle) calculations. In panel (b), the field-free vibrational motion of the Franck-Condon wave packet on the lower potential curve of D_2^+ is presented. The time-dependent density of the nuclear wave packet is displayed by color map. The darker the color, the larger the value of the nuclear density. Additionally, the time-dependent average of the internuclear distance (dashed line) and the time-dependent average of the momentum (dashed-dotted line; scale on the right hand side) are also shown. The solid and the dotted horizontal lines denote the zero momentum (see the scale at the right hand side) and the position of the LICI, respectively. In both panels, dotted vertical lines denote the time delays for which the average of the internuclear distance exhibits an extremal value. In panel (a), the vertical dashed lines denote time delays of 23 fs, 29 fs, and 34 fs.

the dissociation, while the opposite is true if the nuclear wave packet goes backward. In all three cases, the time period of the dissociation yield curves is almost identical, in spite of the fact that they possess a relative phase difference with respect to the field-free vibration. We might explain the appearance of this relative phase as the interplay between the average of the internuclear distance and the average of the momentum values. The greater the positive momentum ($\frac{\hbar}{i}\frac{\partial}{\partial R}$) and the average of the internuclear distance (R), the larger is the expected total dissociation yield. Therefore, the time delay corresponding to the maximum value of the total dissociation yield curve is placed somewhere between the maximum of the average momentum ($\langle\psi(R,t) \mid \frac{\hbar}{i}\frac{\partial}{\partial R} \mid \psi(R,t)\rangle$) and that of the average internuclear distance ($\langle\psi(R,t) \mid R \mid \psi(R,t)\rangle$).

One can see in Figure 2 that the oscillation amplitudes of both the total dissociation yield (panel (a)) and the field-free curves showing the position and momentum averages (panel (b)) decrease. Surprisingly, this decay is much less pronounced

for the total dissociation yield. The initial nuclear wave packet is built up from several vibrational eigenstates and, therefore, after a while, the density of the time evolved system possesses large values well above and below the curve of the mean value of the internuclear distance. But the dissociation mainly takes place from vibrational levels close to the energy of the LICI (see Fig. 3). The vibrational motion of this smaller set of eigenstates remains synchronized to each other for a longer period of time than that of the total wave function. Consequently, their synchronous return to the large internuclear region is longer living than the periodic motion of the mean values. In turn, this phenomenon causes a slower decay in the periodic change of the total dissociation yield compared to the amplitude of the average internuclear distance.

What is also interesting and calls for further investigation is that although the total dissociation yields obtained by chirped pulses display a similar dependence on the delay time as that observed in the TL case, the differences between the maxima and minima are different, or in other words, the dissociation yield oscillates with smaller amplitude as a function of delay time. Both enhanced and suppressed dissociations occur by using a chirped laser pulse depending upon the delay time between the ionization and the applied laser field. Another possible interpretation is that the sweep of the frequency in the chirped pulse diminishes the advantage of perfectly synchronized delay times and reduces the disadvantage of asynchronously timed excitations. Almost the same dissociation yield curves are provided by the negatively and positively chirped laser pulses. This is probably due to the fact that in a given chirped pulse, the frequency changes at $t = t_0$ from smaller (larger) values than ω_0 to larger (smaller) ones. Here, other choices of chirp can be used to determine other scenarios of dissociation.

From Fig. 2 (panel (a)), we see that the 23 fs and 34 fs delay times belong to one of the minima and to the neighboring maximum values of the total dissociation yield curve, respectively, while in between them, at 29 fs delay time, the three different pulses provide nearly the same amount of dissociation yield. For these three different delay times, the computed KER spectra (Eq. (6)) of the D_2^+ photofragments at 1×10^{13} W/cm^2 intensity are displayed in Figure 3. Analyzing these results reveals that there are three distinct groups of vibrational eigenstates of the ion leading to three different regions in the KER spectra. The lowest vibrational eigenstates ($v < 2$) remain practically bonded with these parameters of the laser field — no bond softening happens. In the high energy region ($v > 4$), the bond hardening plays a role. And finally around the energy of the LICI ($v = 2, 3, 4$), we have significant bond softening without the presence of bond hardening. Most of the dissociation takes place in this energy region as can be clearly seen in Fig. 3.

It can be seen that at 23 fs delay time, the total dissociation yield is increased by more than 60% due to the effect of the chirp (see Fig. 2). Its signature is clearly visible in the spectrum as well (Fig. 3(a) panel). In the intermediate KER region, the structure of the energy distribution hardly changes due to the chirp, only the peaks will significantly be higher. The sign of the chirp plays a role only in the large energy region — especially at $v = 7$ and 8 — but its overall effect hardly modifies the total yield. Let us consider now the 34 fs delay time. In this case, due to the effect of the chirp, the dissociation probability decreases by about 10%–15%. Practically, all these decreases can be

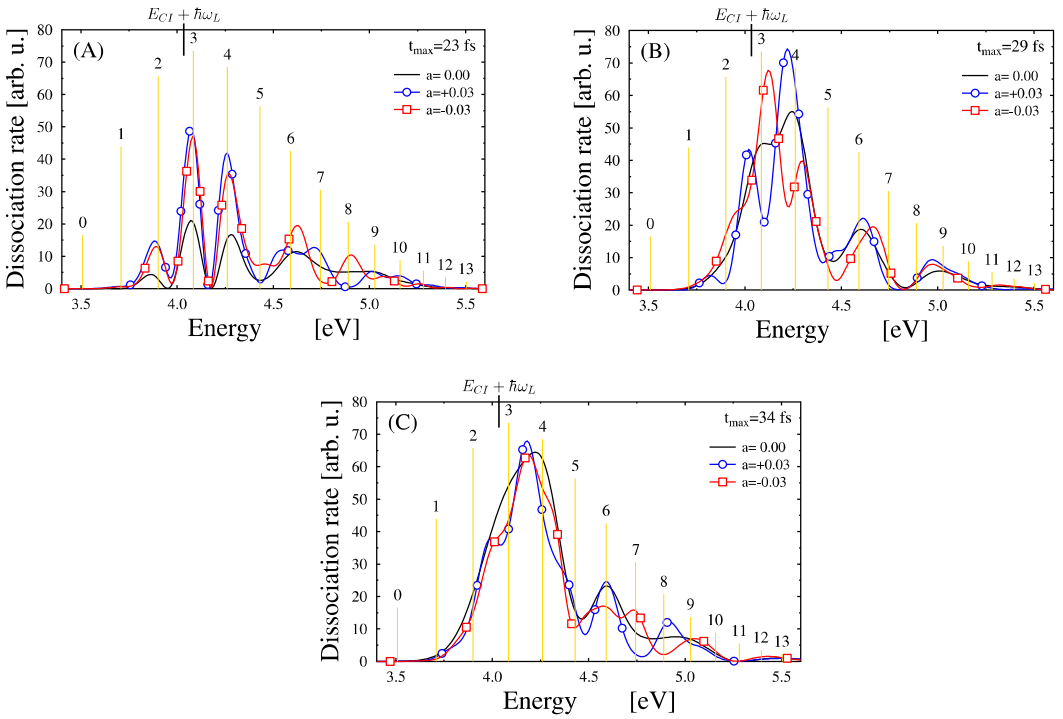

FIG. 3. Kinetic energy release (KER) spectra of the D_2^+ photofragments at 1×10^{13} W/cm^2 intensity. Results are presented for negatively chirped (square) $a = -0.03$, for transform limited (solid line) $a = 0$, and for positively chirped (circle) $a = 0.03$ laser pulses for three different values of delay time. Panels (a), (b), and (c) belong to 23 fs, 29 fs, and 34 fs delay times, respectively. Vertical lines denote the different vibrational levels of D_2^+ in the field-free case shifted by the photon energy ($\hbar\omega_L = 6.199$ eV) and their height is proportional to the norm of the given eigenfunction in the initial FC distribution.

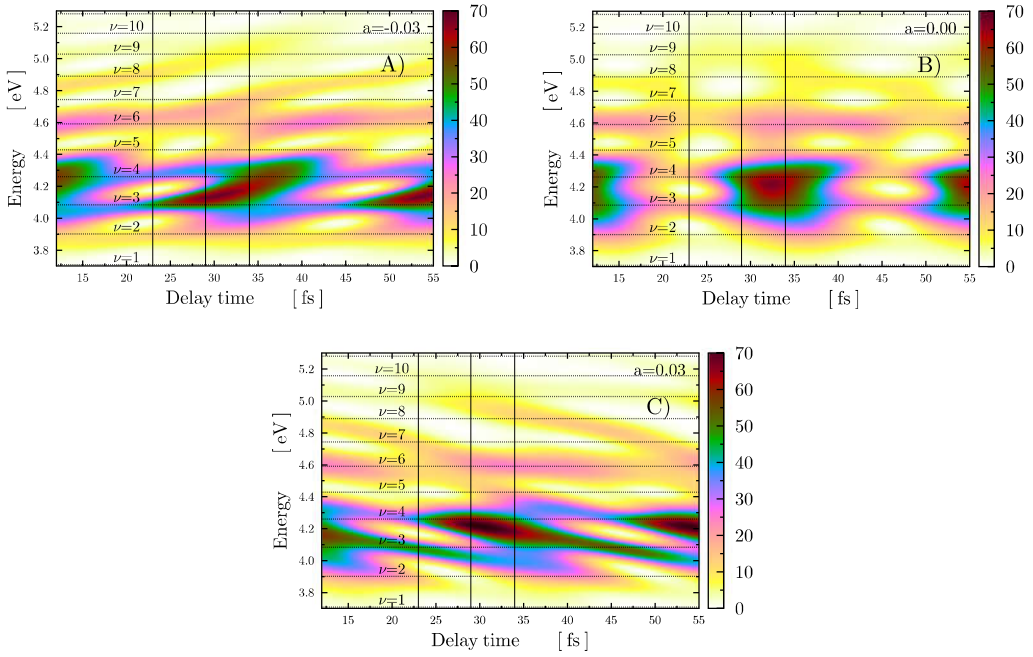

FIG. 4. Kinetic energy of the photofragments of the D_2^+ ion as a function of delay time at 1×10^{13} W/cm^2 intensity. Results are presented for negatively chirped $a=-0.03$ (panel (a)), for transform limited $a=0$ (panel (b)), and for positively chirped $a=0.03$ (panel (c)) laser pulses. Horizontal lines denote the different vibrational levels of D_2^+ in the field-free case shifted by the photon energy ($\hbar\omega_L=6.199$ eV). The vertical lines mark the 23, 29, and 34 delay times.

accounted to the dissociation from two vibrational eigenstates $\nu=3$ and 4. As a signature, the main chirped peak is narrower (Fig. 3, panel (c)). And again, the sign of the chirp plays a characteristic role in the large energy region. To summarize, one can realize measurable difference between the heights of the various spectra in panel (a) at 23 fs time delay and also between the widths of the spectra in panel (c) at 34 fs time delay. The integrated effect of these differences appears then in Figure 2. However, the situation is quite different at 29 fs time delay. For this time delay, the total dissociation yield is practically unaffected by the chirps. In contrast to the total dissociation yield being essentially independent from the chirp at this time delay (Fig. 2), panel (b) of Fig. 3 does show measurable structural changes as a consequence of the chirp. The structure of the curves on this panel is fairly rich considering the simple behavior shown in Figure 2 (panel (a)) from which one would not expect noticeable differences in the impact of the three different pulses. Indeed, there is no measurable difference in the total yield of the dissociation, but the structure of the KER spectra is nevertheless very different. The two spectra obtained by the chirped laser pulses are modulated into different directions in the intermediate KER region ($\nu=2$, 3, 4) comparing them to that obtained by the TL pulse; namely, the positively chirped laser pulse decreases the dissociation yield around $\nu=2$ and 3 and increases it in between these two levels and at $\nu=4$, while the reverse effect holds by changing the sign of the chirp. A similar tendency has been measured in the experimental works of Zajfman and his coworkers[47,54] for H_2^+. On the other hand, at 29 fs time delay, the dependence on the sign of the chirp decreased substantially in the high energy region.

For better visualizing the dependence of the kinetic energy release of the photofragments on the time delay, we collect

TABLE I. Total dissociation probability of the D_2^+ ion as a function of laser intensity computed (2d). Results are presented for transform limited $a=0$, negatively $a=-0.03$, and positively chirped $a=0.03$ situations. For the chirped pulses, the amount of total dissociation rate as well as its ratio to the TL total rate is also presented. The delay time (difference between the time of the sudden ionization of the D_2 molecule and the time corresponding to the maximum value of the laser pulse) is 23 fs. The first minimum of the total dissociation yield curves in Fig. 2 (panel (a)) is at ≈23 fs.

	Time delay = 23 fs				
I_0 (W/cm^2)	$a=0$	$a=-0.03$		$a=+0.03$	
10^9	2.01×10^{-5}	2.99×10^{-5}	148.9%	3.06×10^{-5}	152.4%
10^{10}	1.71×10^{-4}	2.68×10^{-4}	156.7%	2.75×10^{-4}	160.9%
10^{11}	1.67×10^{-3}	2.63×10^{-3}	157.6%	2.70×10^{-3}	161.9%
10^{12}	0.015 76	0.024 90	158.0%	0.025 64	162.9%
10^{13}	0.094 51	0.157 07	166.2%	0.162 12	171.5%
10^{14}	0.278 68	0.430 83	154.6%	0.455 60	163.5%

TABLE II. Total dissociation probability of the D_2^+ ion as a function of laser intensity computed (2d). Results are presented for transform limited $a=0$, negatively $a=-0.03$ and positively chirped $a=0.03$ situations. For the chirped pulses the amount of total dissociation rate as well as its ratio to the TL total rate is also presented. The delay time (difference between the time of the sudden ionization of the D_2 molecule and the time corresponding to the maximum value of the laser pulse) is 34 fs. The second maximum of the total dissociation yield curves in Fig. 2 (panel (a)) is at ≈34 fs.

	Time delay = 34 fs				
I_0 (W/cm^2)	$a=0$	$a=-0.03$		$a=+0.03$	
10^9	6.71×10^{-5}	5.44×10^{-5}	81.0%	5.32×10^{-5}	79.3%
10^{10}	6.41×10^{-4}	5.13×10^{-4}	80.1%	5.02×10^{-4}	78.3%
10^{11}	6.33×10^{-3}	5.07×10^{-3}	80.0%	4.95×10^{-3}	78.3%
10^{12}	0.058 34	0.047 26	81.0%	0.046 23	79.2%
10^{13}	0.330 97	0.289 22	87.4%	0.283 85	85.8%
10^{14}	0.708 34	0.660 95	93.3%	0.660 87	93.3%

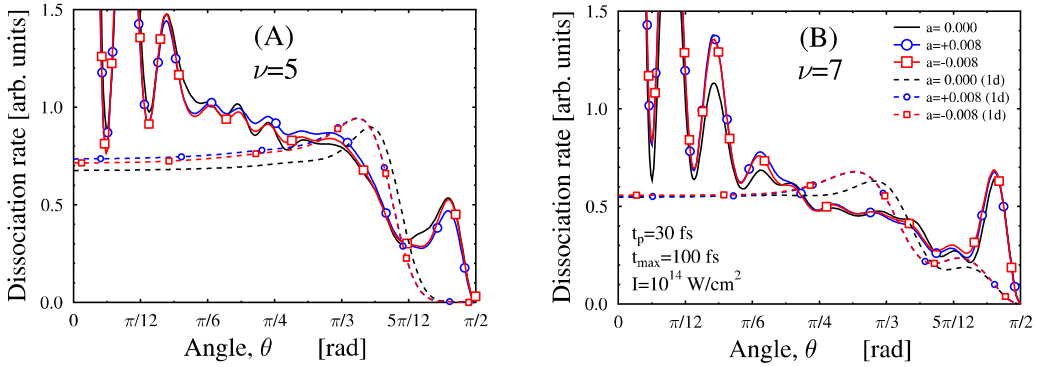

FIG. 5. Fragment angular distributions of the dissociating D_2^+ molecule for two different initial vibrational states ($\nu = 5$, panel (a); $\nu = 7$, panel (b)). Curves are presented both for one dimensional (1d, no LICI situation) and for 2d calculations. The applied field intensity is 1×10^{14} W/cm^2. Shown are the results for the transform limited $a = 0$, negatively chirped $a = -0.008$ (square), and positively chirped $a = 0.008$ (circle) calculations.

in Fig. 4 KER data for three different laser pulses. In the case of the transform limited pulse, the peaks are most pronounced for time delays corresponding to the minima of the total dissociation yields. In between two minima, the peaks remain at the same energetic position but they are higher and strongly overlapping. For the chirped pulses, the main peak of the spectra (peak of largest intensity around $E_{LICI} + \hbar\omega_0$) is narrower compared to the transform limited situation. In the case of negatively chirped pulses, the position of the peaks of the KER spectra is moving towards larger energies as the time delay increases. For the case of the positively chirped pulses, the opposite is true. This slant of the KER peaks plotted against delay time seems to represent an important aspect of the KER distributions. From our current study, it is not clear yet what the underlying processes are.

So far we have not varied the intensity of the laser pulse in the calculations. A laser pulse with the intensity $I = 1 \times 10^{13}$ W/cm^2 was applied. As previously discussed, the strength of the nonadiabatic coupling is determined by the laser intensity. We now present two tables collecting the numerical results for the total dissociation probability for several different laser intensity values ($1 \times 10^9 - 1 \times 10^{14}$ W/cm^2). The results in Table I and in Table II refer to 23 fs and 34 fs delay times, respectively. It was discussed above for $I = 1 \times 10^{13}$ W/cm^2 that at 23 fs delay time the value of the minimum dissociation yield of the TL curve is substantially smaller than that of the chirped curves. This tendency holds for the whole studied interval of the intensities (see Table I). In all three cases, the total dissociation yields increase monotonically as the laser intensity increases between 1×10^9 and 1×10^{13} W/cm^2. Then, at the highest intensity studied (1×10^{14} W/cm^2), the ratio drops again. In Table II, we collected the results for the case of 34 fs delay time. As this value of the delay time provides the largest obtained dissociation probability yields, but at which the ionization is suppressed by using chirped laser pulses. Consequently, the ratios between chirped and TL results are always less than 100%. However, this latter one increases monotonically as the intensity increases.

To further analyze the effect of frequency chirping of laser pulses on the dissociation dynamics of the D_2^+ ion in the LICI picture, we present the angular distribution of the photofragments (Eq. (7)). However, to also cover another relevant situation, we choose as initial condition, the individual vibrational levels ($\nu = 5$ and $\nu = 7$). The results are displayed in Fig. 5. Here, we repeated our former calculations (see Fig. 2B and Fig. 2D in Ref. 11) augmenting them with new results obtained by simulations provided by negatively and positively chirped laser pulses. For this calculation, the pulse parameter was chosen to be ($I = 1 \times 10^{14}$ W/cm^2, $t_{pulse} = 30$ fs). In the case of the TL pulse, only the intensity of the light determines the time dependence of the shape of the adiabatic or light induced potentials. As the intensity is continuously changing during the evolution of the pulse, these surfaces are changing as well. Using chirped laser pulses to initiate the dynamics, the situation becomes a bit more complex, but nevertheless its fingerprint on the final outcome has not changed much. In such a case not only the instantaneous value of the laser intensity but also the instantaneous value of the carrier frequency jointly determines the actual shape of the adiabatic potentials.[10] Therefore, the eigenvalues of the upper adiabatic potentials might shift compared to the TL case. This shift can be smaller or greater depending upon the value of the chirp parameter. In our present situation, the chirp parameters applied do not cause relevant changes on the adiabatic potential energy surface and, therefore, our earlier finding for the direct signature of light induced conical intersections in diatomics[11] also holds for the chirped pulses. The large peaks on the 2d curves — obtained by simulations applying chirped laser pulses — around $\theta \gtrsim 11\pi/24$ appear again. The time dependence of the laser frequency does not suppress or modify significantly the strong nonadiabatic effect induced by the molecular rotation due to the laser field.

For the sake of completeness, 1d calculations have also been performed and shown in Fig. 5. They behave similarly to those of the 1d calculations using the TL pulse. In other words, they fail to describe the 2d reality.

V. CONCLUSIONS

In summary, we have discussed the impact of the LICIs created by frequency chirped laser pulses on the dissociation dynamics of D_2^+ molecule. We concentrated here on linearly chirped pulses. We have found that the amplitude of the periodic change in the total dissociation rate against the delay time is significantly compressed by the chirped pulse compared to the transform limited case. The KER displays more detailed

consequences of the frequency sweeping. These findings as well as those for the angular distributions of the D_2^+ photofragments all show a clear signature of the LICIs. Based on these results, we could also explain the phase difference between the curves of the dissociation yield and the field-free vibration of the nuclear wave packet and also the decay of the oscillation amplitude of the dissociation yield found in the calculations. Nevertheless, the origin of many effects arising due to the chirp of the pulses is not yet clarified. For the in depth understanding and explaining of our current findings, more detailed analysis is required.

In future works, it would be particularly interesting to perform new studies using different pulse lengths while initiating the nuclear dynamics from individual vibrational eigenstates. From these results, we expect to understand clearly the physical phenomena beyond the enhanced and suppressed dissociation processes induced by chirped laser pulses.

ACKNOWLEDGMENTS

The authors acknowledge the financial support by the Deutsche Forschungsgemeinschaft (Project ID CE10/50-2). Á.V. also acknowledges the OTKA (No. NN103251) project. For this work, the supercomputing service of NIIF has been used. This material is based upon work supported by part by the U.S. ARL and the U.S. ARO under Grant No. W911NF-14-1-0383.

[1]N. Moiseyev, M. Sindelka, and L. S. Cederbaum, J. Phys. B **41**, 221001 (2008).
[2]M. Sindelka, N. Moiseyev, and L. S. Cederbaum, J. Phys. B **44**, 045603 (2011).
[3]L. S. Cederbaum, Y. C. Chiang, P. V. Demekhin, and N. Moiseyev, Phys. Rev. Lett. **106**, 123001 (2011).
[4]G. J. Halász, Á. Vibók, M. Sindelka, N. Moiseyev, and L. S. Cederbaum, J. Phys. B **44**, 175102 (2011).
[5]G. J. Halász, M. Sindelka, N. Moiseyev, L. S. Cederbaum, and Á. Vibók, J. Phys. Chem. A **116**, 2636 (2012).
[6]G. J. Halász, Á. Vibók, M. Sindelka, L. S. Cederbaum, and N. Moiseyev, Chem. Phys. **399**, 146 (2012).
[7]G. J. Halász, Á. Vibók, N. Moiseyev, and L. S. Cederbaum, J. Phys. B **45**, 135101 (2012).
[8]G. J. Halász, Á. Vibók, H. D. Meyer, and L. S. Cederbaum, J. Phys. Chem. A **117**, 8528 (2013).
[9]G. J. Halász, Á. Vibók, N. Moiseyev, and L. S. Cederbaum, Phys. Rev. A **88**, 043413 (2013).
[10]G. J. Halász, A. Csehi, Á. Vibók, and L. S. Cederbaum, J. Phys. Chem. A **118**, 11908 (2014).
[11]G. J. Halász, Á. Vibók, and L. Cederbaum, J. Phys. Chem. Lett. **6**, 348 (2015).
[12]H. Köppel, W. Domcke, and L. S. Cederbaum, Adv. Chem. Phys. **57**, 59 (1984).
[13]M. Baer, Chem. Phys. Lett. **35**, 112 (1975).
[14]M. Baer and G. D. Billing, *The Role of Degenerate States in Chemistry*, Advances in Chemical Physics Vol. 124 (Wiley-Interscience, New York, 2002).
[15]*Conical Intersections: Electronic Structure, Dynamics and Spectroscopy*, edited by W. Domcke, D. R. Yarkony, and H. Köppel (World Scientific, Singapore, 2004).
[16]G. A. Worth and L. S. Cederbaum, Annu. Rev. Phys. Chem. **55**, 127 (2004).
[17]M. Baer, *Beyond Born Oppenheimer: Electronic Non-Adiabatic Coupling Terms and Conical Intersections* (Wiley, Hoboken, NJ, 2006).
[18]S. Matsika, Rev. Comput. Chem. **23**, 83 (2007).
[19]S. C. Althorpe, T. Stecher, and F. Bouakline, J. Chem. Phys. **129**, 214117 (2008).
[20]F. Bouakline, Chem. Phys. **442**, 31 (2014).
[21]M. Ben-Nur, F. Molnar, K. Schulten, and T. J. Martinez, Proc. Natl. Acad. Sci. U. S. A. **99**, 1769 (2002).
[22]T. J. Martinez, Nature **467**, 412 (2010).
[23]J. Kim, H. Tao, J. L. White, V. S. Petrović, T. J. Martinez, and P. H. Bucksbaum, J. Phys. Chem. A **116**, 2758 (2012).
[24]P. V. Demekhin and L. S. Cederbaum, J. Chem. Phys. **139**, 154314 (2013).
[25]M. E. Corrales, J. González-Vázquez, G. Balerdi, I. R. Solá, R. de Nalda, and L. Bañares, Nat. Chem. **6**, 785 (2014).
[26]I. R. Solá, J. González-Vázquez, R. de Nalda, and L. Bañares, Phys. Chem. Chem. Phys. **17**, 13183 (2015).
[27]A. Zavriyev, P. H. Bucksbaum, H. G. Muller, and D. V. Schumacher, Phys. Rev. A **42**, 5500 (1990).
[28]A. D. Bandrauk and M. Sink, Chem. Phys. Lett. **57**, 569 (1978).
[29]A. D. Bandrauk and M. Sink, J. Chem. Phys. **74**, 1110 (1981).
[30]E. E. Aubanel, J. M. Gauthier, and A. D. Bandrauk, Phys. Rev. A **48**, 2145 (1993).
[31]E. Charron, A. Giusti-Suzor, and F. H. Mies, Phys. Rev. A **49**, R641 (1994).
[32]S. Chelkowski, T. Zuo, O. Atabek, and A. D. Bandrauk, Phys. Rev. A **52**, 2977 (1995).
[33]A. Giusti-Suzor, F. H. Mies, L. F. DiMauro, E. Charron, and B. Yang, J. Phys. B **28**, 309 (1995).
[34]R. Numico, A. Keller, and O. Atabek, Phys. Rev. A **52**, 1298 (1995).
[35]I. Sánchez and F. Martín, Phys. Rev. A **57**, 1006 (1998).
[36]K. Sandig, H. Figger, and T. V. Hansch, Phys. Rev. Lett. **85**, 4876 (2000).
[37]V. N. Serov, A. Keller, O. Atabek, and N. Billy, Phys. Rev. A **68**, 053401 (2003).
[38]J. H. Posthumus, Rep. Prog. Phys. **67**, 623 (2004).
[39]V. N. Serov, A. Keller, O. Atabek, H. Figger, and D. Pavidic, Phys. Rev. A **72**, 033413 (2005).
[40]M. Uhlmann, T. Kunert, and R. Schmidt, Phys. Rev. A **72**, 045402 (2005).
[41]P. Q. Wang *et al.*, Phys. Rev. A **74**, 043411 (2006).
[42]F. Anis and B. D. Esry, Phys. Rev. A **77**, 033416 (2008).
[43]F. Anis, T. Cackowski, and B. D. Esry, J. Phys. B: At. Mol. Opt. Phys. **42**, 091001 (2009).
[44]J. J. Hua and B. D. Esry, Phys. Rev. A **80**, 013413 (2009).
[45]S. Adhikari *et al.*, J. Phys. Chem. A **113**, 7331 (2009).
[46]A. K. Paul, S. Adhikari, M. Baer, and R. Baer, Phys. Rev. A **81**, 013412 (2010).
[47]V. S. Prabhudesai, U. Lev, A. Natan, B. D. Bruner, A. Diner, O. Heber, D. Strasser, D. Schwalm, I. Ben-Itzhak, J. J. Hua, B. D. Esry, Y. Silberberg, and D. Zajfman, Phys. Rev. A **81**, 023401 (2010).
[48]U. Thumm, T. Niederhausen, and B. Feuerstein, Phys. Rev. A **77**, 063401 (2008).
[49]M. Fischer *et al.*, New J. Phys. **13**, 053019 (2011).
[50]M. Fischer, U. Lorenz, B. Schmidt, and R. Schmidt, Phys. Rev. A **84**, 033422 (2011).
[51]J. McKenna, F. Anis, A. M. Sayler, B. Gaire, N. G. Johnson, E. Parke, K. D. Carnes, B. D. Esry, and I. Ben-Itzhak, Phys. Rev. A **85**, 023405 (2012).
[52]H. X. He, R. F. Lu, P. Y. Zhang, K. L. Han, and G. Z. He, J. Chem. Phys. **136**, 024311 (2012).
[53]Y. Furukawa, Y. Nabekawa, T. Okino, A. A. Eilanlou, E. J. Takahashi, P. Lan, K. L. Ishikawa, T. Sato, K. Yamanouchi, and K. Midorikawa, Opt. Lett. **37**, 2922 (2012).
[54]A. Natan, U. Lev, V. S. Prabhudesai, B. D. Bruner, D. Strasser, D. Schwalm, I. Ben-Itzhak, O. Heber, D. Zajfman, and Y. Silberberg, Phys. Rev. A **86**, 043418 (2012).
[55]F. V. Bunkin and I. I. Tugov, Phys. Rev. A **8**, 601 (1973).
[56]S. I. Chu, C. Laughlin, and K. Datta, Chem. Phys. Lett. **98**, 476 (1983).
[57]D. B. Milosevic, G. G. Paulus, D. Bauer, and W. Becker, J. Phys. B **39**, R203 (2006).
[58]H. D. Meyer, U. Manthe, and L. S. Cederbaum, Chem. Phys. Lett. **165**, 73 (1990).
[59]U. Manthe, H. D. Meyer, and L. S. Cederbaum, J. Chem. Phys. **97**, 3199 (1992).
[60]M. H. Beck, A. Jäckle, G. A. Worth, and H. D. Meyer, Phys. Rep. **324**, 1 (2000).
[61]G. A. Worth *et al.*, The MCTDH package, version 8.2, University of Heidelberg, Heidelberg, Germany, 2000; H. D. Meyer , The MCTDH package, versions 8.3 and 8.4, University of Heidelberg, Germany, 2002 and 2007, http://mctdh.uni-hd.de/.
[62]H. D. Meyer, F. Gatti, G. A. Worth *et al.*, *Multidimensional Quantum Dynamics: MCTDH Theory and Applications* (Wiley-VCH, Weinheim, Germany, 2009).
[63]V. S. Malinovsky and J. L. Krause, Eur. Phys. J. D **14**, 147 (2001).
[64]A. Datta, S. S. Bhattacharyya, and B. Kim, Phys. Rev. A **65**, 043404 (2002).